Null test optics for the MMT and Magellan 6.5-m *f*/1.25 primary mirrors

J. H. Burge, D. S. Anderson, D. A. Ketelsen, and S. C. West

Steward Observatory Mirror Lab
University of Arizona
Tucson, Arizona 85721

ABSTRACT

The instruments used to interferometrically measure the optical surfaces of the 6.5-m *f*/1.25 primary mirrors for the MMT conversion and Magellan Telescopes must compensate over 800 μm surface departure from the best fitting sphere. The errors in the optical test must not contribute more than 0.04 arc seconds FWHM to the final image and the conic constant must be held to 0.01%. This paper presents the design, analysis, fabrication, and certification of the instruments used to measure these giant mirrors to such high accuracy.

1. INTRODUCTION

Primary mirrors for modern telescopes are tested interferometrically from the center of curvature using null correctors (see Fig. 1). The null corrector, or null lens, compensates for the asphericity of the mirror surface. Interferometric testing with a null lens allows an accurate, high-resolution measurement of the entire surface that can be made in several minutes. Two instruments are being built for interferometric measurements of the 6.5-m mirrors at the Steward Observatory Mirror Lab (SOML). An infrared interferometer with a germanium and ZnSe null corrector will test the ground surface to monitor loose-abrasive grinding. The polished surface will be measured with green laser light using a Shack cube interferometer co-aligned with a BK7 null corrector. Both the infrared and visible systems have been carefully designed to give excellent performance in terms of wavefront correction, alignment sensitivity, imaging of the mirror to the detector, diffraction effects, ghost reflections, and ease of use. The lenses for these instruments are fabricated and measured precisely. The accurate alignment and stable support of these lenses require a well designed and constructed mechanical system. The mounting and alignment methods used for the new null correctors follow from the experience of building similar, smaller instruments at Steward Observatory.[1]

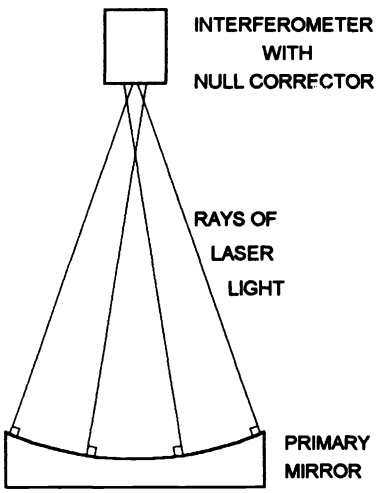

Figure 1. Schematic drawing of null test.

An optical test for measuring null correctors has been developed that uses a rotationally symmetric computer-generated hologram (CGH) to synthesize the wavefront that would be reflected by a perfect primary mirror. The test of a null lens is performed by measuring the CGH through the null corrector. Since the CGH is made independently from the null corrector, agreement between the null lens and the CGH indicate that both the null lens and the CGH are correct. This test is planned for both null correctors for the 6.5-m mirrors.

0-8194-1494-8/94/$6.00

2. INTERFEROMETRIC METROLOGY USING NULL CORRECTORS

2.1 DESCRIPTION OF NULL TEST

The interferometric null test uses interference between light that has been reflected from the mirror, and light from a reference surface. The interferometer creates a spherical wavefront of laser light that is split into a reference and a test beam. The test beam travels through the null corrector, reflects off the mirror under test, and travels back through the null corrector into the interferometer. The test is autostigmatic -- the light retraces its path to form a point image coincident with the source point. The reference beam is reflected off a high-quality spherical or plano surface. The test beam is recombined with the reference beam causing an interference fringe pattern that corresponds to the difference between the two wavefronts. The fringe pattern is imaged onto a detector for analysis. By simultaneously shifting the reference beam and measuring the change in intensity at each pixel of the image, the phase difference, which is proportional to the surface error of the mirror, is calculated at each sampled location.

The null corrector is designed to modify the spherical wavefront from the interferometer to produce a wavefront that matches the desired aspheric shape of the mirror. If both the null lens and the mirror are perfect, this test wavefront will exactly match the reference wavefront. The resulting interference pattern will show no variation, giving a "null" result (no surface error). If the mirror does have figure errors, they will be imparted to the reflected wavefront and show up in the interference pattern. Errors in the reflected wavefront are exactly twice the size of the errors in the mirror. It is important to note that any error in the null corrector will cause a shape change in the test wavefront that will be interpreted as a figure error in the mirror. The null test simply measures how well the mirror fits the template created by the null corrector. It requires additional testing to determine the absolute accuracy of this template.

Of the several types of null correctors shown in Fig. 2, the Offner null lens is most commonly used for large modern primary mirrors because it allows the measurement of fast primaries to high accuracy and with reasonable manufacturing tolerances. This null corrector consists of a large relay lens and a smaller field lens. The design principle of the null corrector uses the field lens to image the primary mirror onto the relay lens. The power and shape of the relay lens are chosen to introduce spherical aberration that compensates the asphericity of the primary mirror. The optimization of the two-element Offner null corrector is discussed by Offner[5], Holleran[6], Puryaev and Shandin[7], Moya and Landgrave[8], Sasian[9,10], DeVoe[11], Offner and Malacara[12], and Shafer[13].

The design of the null test requires more than an accurate null corrector. The instruments are complex optical systems with illumination, wavefront correction, and imaging optics. The wavefront correction is performed by the null lens. The illumination optics project a laser beam through a spatial filter to give a well-conditioned wavefront. The imaging optics project the interference pattern as a scaled image of the primary mirror onto the detector plane.

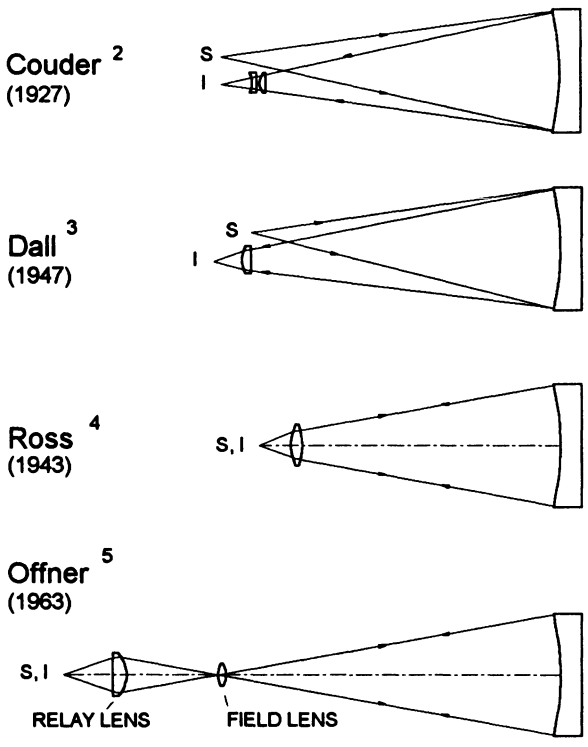

Figure 2. Types of refractive null correctors used for testing primary mirrors.[2,3,4,5] These drawings are schematic and not to scale.

2.2 IMAGING REQUIREMENTS

During grinding and polishing, the data from the infrared and visible interferometers are used to direct the figuring. It is important to minimize the mapping distortion of the mirror through the null lens. The imaging distortion causes two problems in the data analysis; it causes small surface defects to appear shifted radially and it re-maps low order errors from alignment (focus, and coma) into higher order errors. A discussion of interferometric measurement errors introduced by small amounts of distortion is given by Selberg[14] and the details of the effects of

distortion in the null test are given by Burge[1]. The infrared null lens was designed to have minimal mapping error and the visible system uses relay optics to correct the distortion introduced by the null lens.

Improper imaging causes diffraction "ripples" in the measured phase and causes the edge of the mirror to appear flawed. This effect, and other errors from diffraction, are minimized by focusing the mirror onto the detector array. Both of the interferometers use apertures at intermediate images of the primary to help define the focus. Also, a rotating ground glass disk correctly positioned in the visible system eliminates Fresnel noise, which is caused by scatter of the coherent laser light from dust on the lens surfaces. Both null correctors were designed to avoid ghost reflections that can cause troublesome spurious fringes.

2.3 ALIGNMENT OF TEST OPTICS WITH PRIMARY MIRROR

Since this is an autostigmatic test, the shape of the wavefront created by the null corrector defines the shape of the mirror. For a given null lens and spacing to the primary mirror, the shape of the mirror is fully determined by the shape of the wavefront. It is easy in practice to align the null lens with respect to the mirror because the different alignment degrees of freedom cause distinct changes in the interference pattern. To find the correct null lens position and orientation with respect to the mirror, the null lens is first positioned approximately to get the light to reach the detector. Fine adjustments are made to eliminate the fringes of tilt, focus and coma. Interferograms of these characteristic aberrations are shown in Fig. 3. Lateral translation of the null lens causes straight tilt fringes in the interferogram. Vertical translation along the axis causes focus in the interferogram. Rotation of the null corrector about the paraxial center of curvature causes coma in the interferogram. Since it is easy to differentiate tilt, coma, and focus in an interferogram by inspection, the alignment is done quickly and easily.

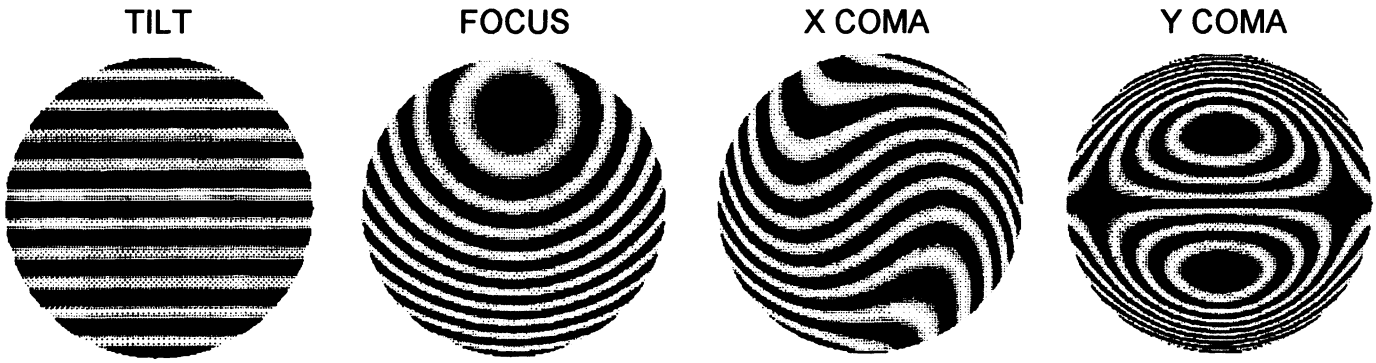

Figure 3. Interferograms showing alignment errors of tilt, focus, and coma. Some tilt has been added to the focus and coma.

A small amount of residual alignment error always exists and must be removed in the data analysis. About a tenth of a fringe of tilt, focus, or coma often remains after alignment. Any small mechanical instabilities will also cause small variations of these aberrations. Since tilt, focus, or coma measured in the mirror comes from test misalignment and because these aberrations do not affect the telescope operation, they are always removed in the data analysis. These low-order terms are easily removed by first fitting Zernike polynomials to the raw data and then subtracting the appropriate terms from the data.

A tolerance is imposed on the primary radius of curvature to insure that the null lens is used at the correct distance from the primary mirror. The null corrector creates a wavefront that propagates to fit the desired shape of the mirror. Since the wavefront changes as it propagates, there is a family of different surfaces that will give a null test, only one of which has the desired shape. Each member of the family can be described to fourth-order in radial position r by specifying a radius of curvature R and conic constant K. In practice, the null lens is moved axially to eliminate power in the reflected wavefront. The distance at which this condition is satisfied depends on R. Therefore the conic constant of the surface matching the wavefront depends on R. The change in K is related to the change in R by

$$\frac{\Delta K}{K} = -\frac{\Delta R}{R}. \tag{1}$$

The radius of curvature R is inferred from a direct measurement of the distance between the null corrector and the primary mirror. The optician monitors this distance and designs the grinding and polishing strokes to keep the radius within tolerance.

The null test is also insensitive to optical surface decentration and tilt with respect to the axis defined by the null corrector. These pose no real problem as long as the decentration and wedge of the optical surface with respect to the 6.5-m blank are less than 1 mm, which can be accommodated in the telescope. The wedge is measured by rotating the mirror about the mechanical reference axis, and measuring runout in the optical surface. The decentration is determined from the amount of coma seen in the null test when the mirror is rotated about is mechanical axis. The centration and wedge of the optical surface are largely determined during generating. Since little material is removed during grinding and polishing, only small changes are made in the mechanical properties of the mirrors.

2.4. ENVIRONMENTAL EFFECTS

Since the measurements of the optical surfaces are performed using instruments many meters away, environmental effects can cause significant errors. Variations in air density can cause both random and systematic errors. Motion of the interferometer or the mirror due to vibration makes phase shifting interferometry difficult and introduces random errors in the measurement. The random errors are reduced to an acceptable level by averaging many measurements, but systematic errors remain and degrade the test accuracy.

The random testing errors are minimized by the design of the test facility and further reduced by averaging. Vibration and air motion (seeing) are the dominant sources of random variations in the testing of large optics. These errors are kept as small as possible by using a large, well-controlled lab and vibration-isolated test tower. The remaining random measurement errors are reduced by averaging large numbers of measurements. The error in the average due to the random, uncorrelated effects decreases as the square root of the number of measurements in the average.

Measurement errors due to vibration are minimized by using an isolated test tower, short integration times, and testing on a null fringe. The testing of primary mirrors at Steward Observatory is performed on a rigid test tower that is isolated from ground vibrations by pneumatic supports (see Fig. 4). This test tower is 24 meters tall and weighs 400 tons. It moves as a rigid body with a resonance of about 1.2 Hz, and lowest internal mode is at 9.5 Hz. The tower isolation reduces the vibration problem to a level that allows phase shifting interferometry, although with some difficulty. The use of a shuttered CCD camera that captures images using very short exposures freezes out fringe vibration during each frame. However, the relative motion between the mirror and the interferometer between frames introduces a measurement error. The error in the phase computation due to vibration is roughly proportional to the spatial phase variation of the surface under test. For a good surface with the system aligned on null fringe, the test surface shows very little spatial variation so the effects of vibration are minimized. A great attribute of the null test is that the testing becomes more accurate as the figure of the mirror improves.

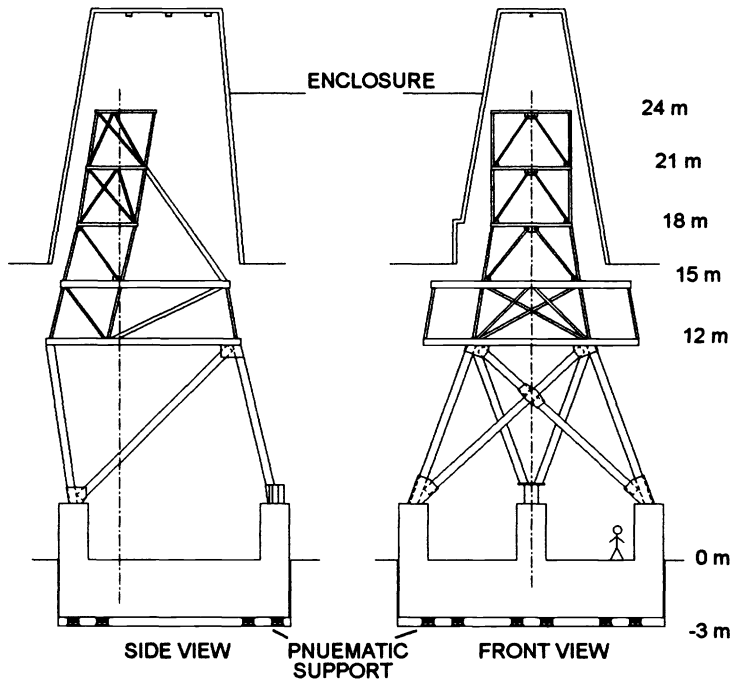

Figure 4. Isolated test tower at Steward Observatory Mirror Lab. The entire 400-ton concrete and steel structure is supported by 40 air-filled isolators. Drawing by E. Anderson.

The atmospheric seeing, or wavefront distortion due to air motion, causes random errors in the surface measurement. Air has refractive index variations proportional to density, thus temperature fluctuations. If a mass of cold, dense air floats over the mirror during a test, the test wavefront will be dis-

torted and the measurement of the surface will indicate a low area on the mirror. The tendency to form these air masses is minimized by using a large lab with well-mixed air and minimal heat (or cold) loading. Eliminating the seeing problem by performing the test in a vacuum chamber[15,16] would be extremely expensive and difficult to implement for large mirrors.

An important point demonstrated by Martin *et al.*[17] is that the random testing errors are distributed where the mirror specification has room for them. The mirror specification allows larger errors at low spatial frequency than high frequency. The random testing errors tend to have mainly low frequency variation while the final mirror surface has very little large-scale variation. The combination of the surface errors at small scales and the measurement errors at large scales easily meets the telescope requirements.

The random seeing averages out, but there may also be systematic density variations that would lead to erroneous measurements. Once the air handlers in the room are turned off, any warm air rises creating a stable vertical gradient. Also, a heat source on one side of the room will cause a stable horizontal density gradient. The effect of the horizontal gradient is measured by rotating the mirror, but there is no such test for the vertical gradient.

The vertical stratification of the air causes a focal length change and a small amount of spherical aberration or change in conic constant. To quantify the effect of a vertical gradient, a computer simulation of the null test was performed, modeling the refractive index gradient of the air using discrete steps. The null test for the 6.5-m $f/1.25$ primary was simulated, setting the number of steps to be large enough that a further decrease in step size did not change the result. Assuming a perfect null corrector at the correct spacing, the resulting power and spherical aberration cause a change in the primary radius R and conic constant K of

$$\Delta K \cong -3.5 \cdot \Delta n$$
$$\frac{\Delta R}{R} = \frac{\Delta n}{2} \tag{2}$$

where Δn = total refractive index difference (mirror to null lens).

The temperature at SOML was measured to have a variation of about 0.5° C from the tower to the shop floor. Since the refractive index of air changes by 1.0×10^{-6} per °C[18], the temperature gradient at SOML causes a conic constant error of less than 2 ppm (parts-per-million) and a radius error of less than 0.3 ppm. Even if this effect was several times more severe, it would remain negligible compared to the null corrector uncertainty of 80 ppm.

A different thermal effect is possible where the deep dish formed by the fast primary mirror holds a stable layer of cool air. A ray-trace simulation of this effect leads to

$$\Delta K \cong -4\Delta n$$
$$\frac{\Delta R}{R} = \Delta n \tag{3}$$

where Δn is the refractive index of the air held in the mirror. This effect is minimized by allowing air to flow through the center hole of the mirror.

3. NULL CORRECTOR FOR FIGURE MEASUREMENTS USING INFRARED LIGHT

An infrared null corrector has been fabricated that uses germanium and ZnSe lenses with a single diamond-turned aspheric surface. The null corrector, shown in Fig. 5, consists of three lenses: an aspheric ZnSe diverger, a plano-convex germanium relay lens, and a plano-convex ZnSe field lens. The optical design uses the aspheric surface to give a near-perfect wavefront error of 0.0014 λ rms and mapping error less than 1.3%. The aspheric surface for this null corrector was diamond turned and measured with a profilometer. The surface deviates from the best-fit sphere by 160 μm and was determined to be correct to ±0.2 μm. The null corrector will be mounted horizontally and aligned to the collimated output from a Twyman-Green interferometer. The interferometer uses a CO_2 laser operating at 10.6 μm, a PZT-shifted reference mirror, and a pyroelectric vidicon detector.[19]

The relative alignment between the system and the primary mirror will be performed by translating the interferometer-null corrector in three directions and steering the beam with a fold flat. The fold flat is positioned 2/3 of the distance from the paraxial to the marginal focus, so tilting the mirror causes a change in pure Zernike coma.

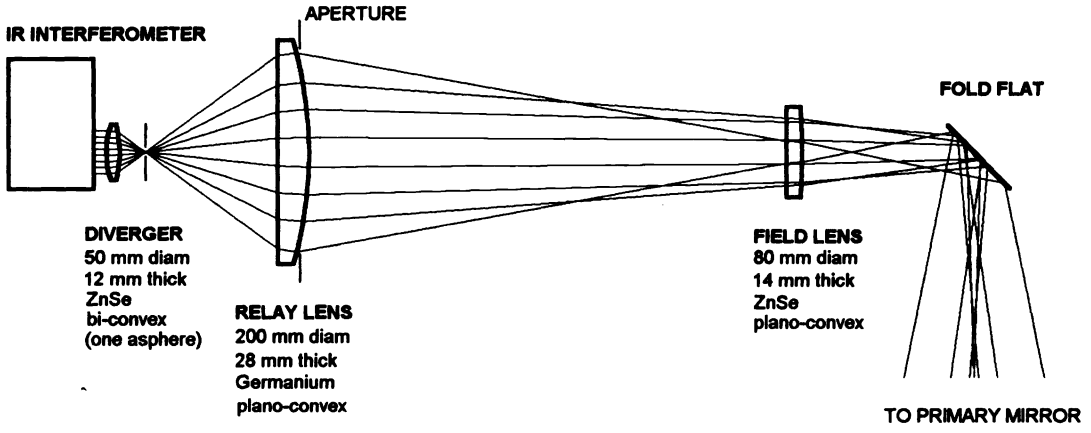

Figure 5. Infrared null corrector for the testing of a 6.5-m *f*/1.25 paraboloidal primary mirrors. This design is optimized for wavefront correction, imaging distortion, alignment tolerances, and ghost reflections.

This null corrector was designed to give excellent imaging performance with no troublesome ghost reflections. In order to avoid the diffraction problems associated with infrared interferometry, the image of the primary mirror is carefully focused onto the vidicon detector. To facilitate this, the null corrector creates a real image of the primary mirror very near the large relay lens, where a circular aperture will be accurately placed to provide a sharp aperture to define the focus. To minimize ghost reflections, the null lens was designed to avoid surfaces with near-normal ray incidence.

The elements in this null lens are the smallest that will work when aligned to machine tolerances (±50 μm over 200 mm). The lenses were carefully made free of wedge so that they can be mounted in a simple accurately machined cell for alignment and spacing. A thorough tolerance analysis of the system indicates that the null lens will contribute surface measurement errors of 1.5 μm rms. Most of this error is due to refractive index inhomogeneity of the large germanium lens. The uncertainty of the conic constant in this null lens due to the manufacturing tolerances is ±0.00016, nearly meeting the final telescope specification of ±0.0001. We plan to check the quality of the entire null lens assembly with a computer-generated hologram.

4. NULL CORRECTOR FOR FIGURE MEASUREMENTS USING VISIBLE LIGHT

4.1 OPTICAL DESIGN

A visible null corrector with a sophisticated imaging system is being built for measuring the 6.5-m *f*/1.25 primary mirrors. The interferometer uses a frequency doubled YAG laser operating at 532 nm, a PZT-shifted Shack cube interferometer, imaging optics, and shuttered CCD detector. The Shack cube, null lens, and imaging optics will be precisely aligned on a single rigid truss. The laser light will be fed into the system through a single mode optical fiber.

The Shack cube interferometer[20] is used because of its simplicity and ease of alignment. The Shack cube, shown in Fig. 6, is fabricated with a small pinhole at the center of curvature of the reference surface. The mechanical alignment of the cube to the null corrector requires only that this one spherical surface be in the correct place. The interferometer is phase shifted by driving the cube and objective with PZT actuators.[21] The Shack cube and null corrector are easily

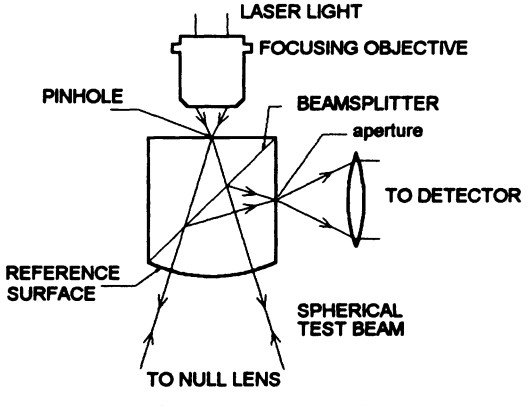

Figure 6. The Shack cube interferometer.

integrated into a single rigid unit.

The null corrector shown in Fig. 7 consists of the Shack-cube and three BK7 lenses: a relay lens, and two field lenses. The optical design gives a wavefront error of 4 nm rms (Fig. 7) and maximum mapping error of almost 5%. The null corrector will be mounted vertically to precise tolerances using the method described by West *et al.*[22] The relative alignment between the system and the mirror will be performed by translating the entire unit in three directions and rotating about two flex-pivot axes. As in the IR test, the lateral rotation is performed about an axis 2/3 of the way from paraxial to marginal focus to decouple wavefront tilt from the alignment. The test alignment will be controlled from a remote testing station.

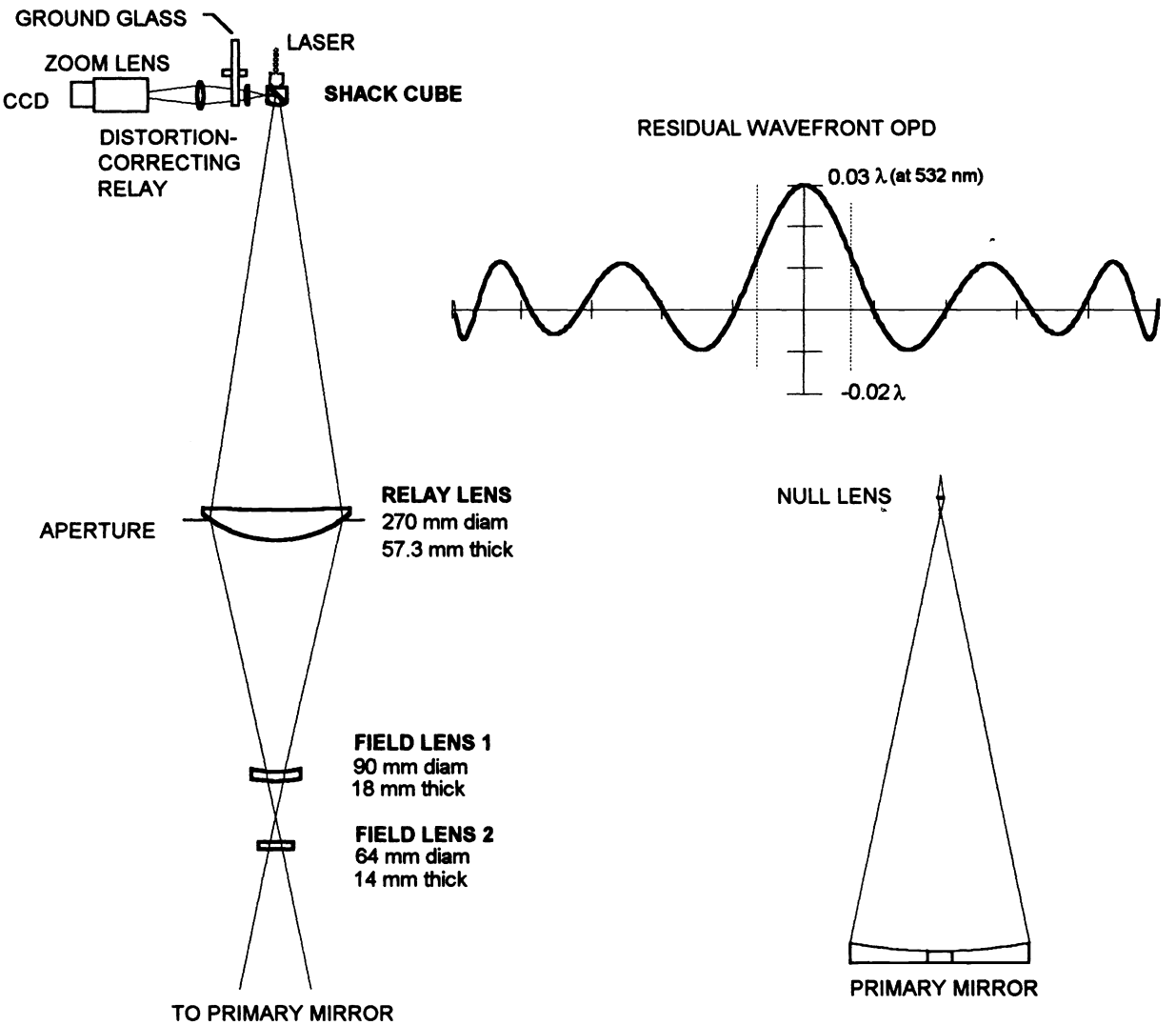

Figure 7. Optical layout of the visible null lens for 6.5-m *f*/1.25 primary mirrors with Shack cube interferometer and distortion-correcting relay. The insets show the residual wavefront and the scale of the null lens with the 6.5-m mirror.

The imaging distortion induced by the null lens is corrected with the relay optics that are shown in Fig. 7. A plot of the mapping error is shown in Fig. 8. This two-lens relay not only corrects the mapping error, but it projects the image of the primary to infinity. This allows the use of a standard zoom lens to re-image the pupil at varying magnification. The re-imaging system consists of a 6X zoom lens fixed to the CCD camera that is mounted on a tip-tilt stage. All of the controls will be operated remotely to allow the optician to magnify the image and to look with increased resolution anywhere on the mirror. High resolution (~6 mm pixels at the mirror) will then be attained for sub-aperture testing without increasing the array size.

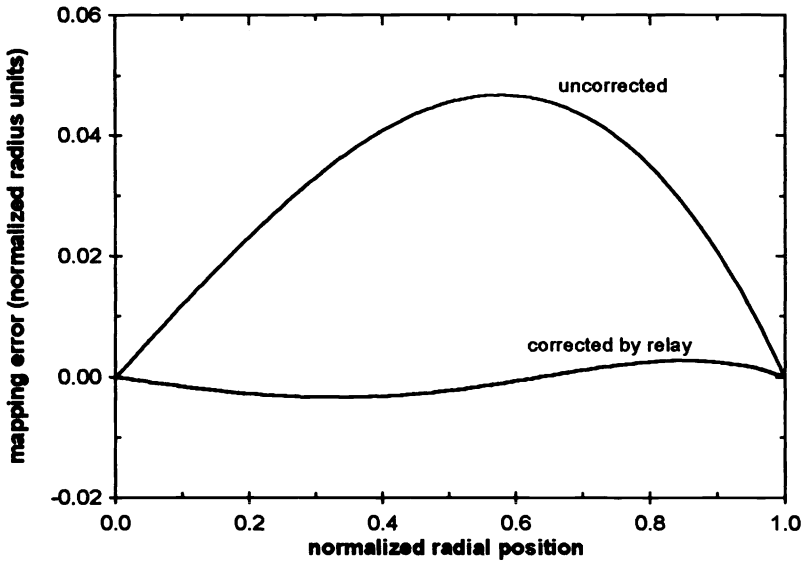

Figure 8. Mapping error for the null lens for testing the 6.5-m *f*/1.25 primary mirror.

4.2 FABRICATION OF VISIBLE NULL CORRECTOR

The lenses, which are made from H5 quality BK7 glass (from Ohara and Schott), are being figured to high quality at Steward Observatory. The spherical surfaces are measured using phase shifting interferometry and the radii are measured using a Fizeau interferometer and lens bench. The lenses are fabricated and measured to a few microns, then the spacings are re-optimized based on the as-fabricated lens dimensions.

The fast surface of the relay lens is measured using a test plate with an interesting illumination scheme shown in Fig. 9. The concave test plate is measured using a Fizeau interferometer with an *f*/0.6 diverger. The diverger reference surface quality is determined by measuring a precision ball at many rotation angles. The convex surface of the relay lens is then measured with this test plate using the Fizeau and diverger only for illumination and imaging. An imaging element is fit to the relay lens with the outer surface nearly concentric with the test plate. For the relay lens measurement, there are four nearly concentric surfaces. To avoid spurious fringes, the Fizeau reference and the imager surface are tilted and the reflections from these surfaces are blocked. The test plate is pushed and phase shifting interferometry is used to allow a high resolution measurement.

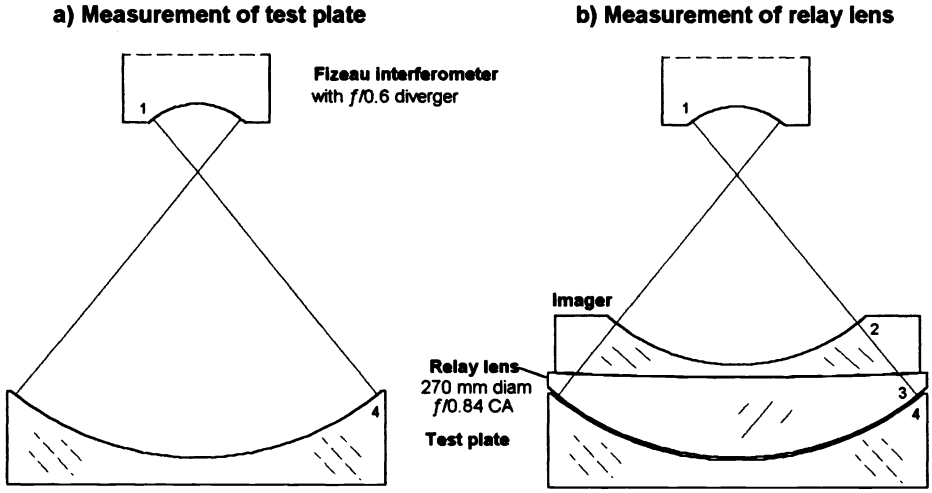

Figure 9. Measurement of the fast convex surface on the relay lens using a test plate. a) The concave test plate is measured using a Fizeau interferometer. b) The fast convex surface (3) is measured against the test plate (4). For this measurement, surfaces 1 and 2 are tilted so the reflections from these surfaces can be blocked.

The performance of the null test requires accurate and stable alignment of the lenses. The alignment procedure used at Steward Observatory for null correctors for highly aspheric mirrors is described by West *et al.* (1992). Using this method, the null lens is aligned onto an Invar frame that provides stability and rigidity. The entire null lens is rotated about a precisely maintained axis and the runout (or wobble) of each surface is mechanically measured and reduced to less than 5 μm. The spacings between the elements are measured using special metering rods and set to an accuracy of about 3 μm. The rigid assembly is mounted to a set of stages that provide translation in *x, y,* and *z* and rotation about the lateral axes for alignment to the primary mirror. A layout of a previously built null corrector for a 3.5-m mirror is shown in Fig. 10.

The null corrector for the 6.5-m mirrors will be much stiffer that those for the 3.5-m mirrors to reduce problems with vibration. It will be supported at a stiff point in the test tower for the same reason. Additionally, we are also pursuing two methods of testing in the presence of vibration: using a fast camera to take the data quickly enough to freeze out the vibration, and an active fringe tracker.

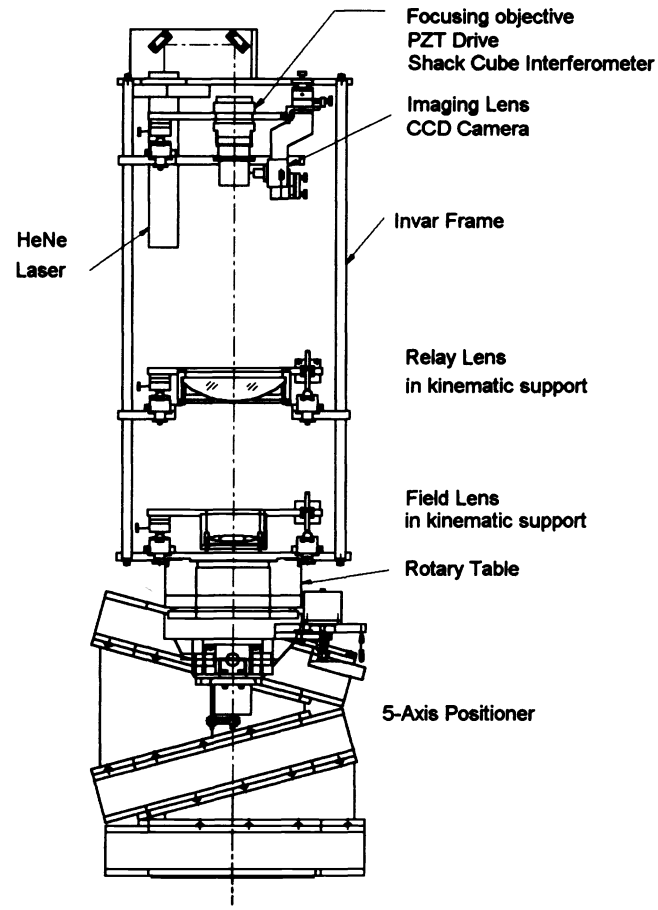

Figure 10. Optomechanical layout of an integral null lens with laser source, phase shifting Shack cube interferometer, imaging system, and 5-DOF positioner. Drawing by D. Murguic.

4.3 TOLERANCE ANALYSIS

Since the null corrector is used as a reference for fabricating the primary mirrors, a thorough tolerance analysis is required to determine the expected accuracy of the test. In this analysis, a table of sensitivities is created showing the performance degradation for small null lens errors, as determined by computer simulation. The effects of the surface figure irregularity and refractive index inhomogeneity are calculated directly (See Table 1). For small errors, the system degradation is assumed to vary linearly with the errors. The sensitivities are then multiplied by expected errors to compute the degradation in system accuracy. This information was used to adjust the tolerances based on the fabrication and alignment process and the required system performance.

Table 1. Contribution to wavefront from surface figures and index inhomogeneity.

Source	Amount	Typical value	Wavefront contribution (rms)
Shack cube rms surface irregularity	ΔS_{SC}	6 nm	$2\,\Delta S_{SC}$
Lens rms surface figure	ΔS_L	8 nm	$2\,(n\text{-}1)\,\Delta S_L$
Lens rms index inhomogeneity	Δn	0.12×10^{-6}	$2\,\Delta n \times thickness$

Since the specification on the primary mirror is in terms of structure functions,[23] the error analysis of the null corrector also uses the functions. The tolerance analysis of the interferometric test was performed by computing structure functions for all of the independent parameters in the system and adding them[1]. Structure functions derived from direct dimensions (spacings, curvatures, refractive index, misalignments, etc.) were computed by ray-trace simulation and analysis of the system. Structure functions from the surface figures of the optical elements were estimated using data from finished optical surfaces. Refractive index inhomogeneity structure functions were estimated for H5 quality glass using melt data and assuming a linear dependence of rms phase difference on point separation. The structure functions from all parameters in the null test are added to give the total test optics structure function. The analysis does not take into account the ability to measure and remove errors in the null lens using the CGH null lens test.

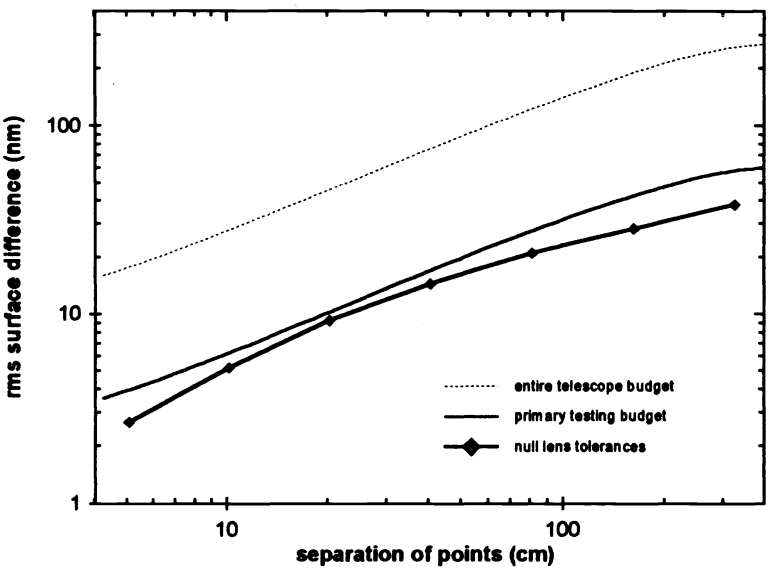

Figure 11. Structure function from the error analysis of the visible null corrector for the 6.5-m *f*/1.25 primary. The telescope and test optics specifications are based on a tilt-corrected Kolmogorov model of the atmosphere with a relaxation at small spatial scales.

The telescope error budget allots primary mirror testing a structure function corresponding to r_0 of 270 cm with 0.04 arc-sec FWHM atmospheric seeing. The tolerance analysis shows that the null corrector will meet this at all spatial scales, with a net uncertainty in the measurement of 21 nm rms. The resulting structure function for the null lens optics is shown in Fig 11.

Distinct from the structure function requirement is a tolerance on the conic constant of the primary. The null lens described introduces an uncertainty of the conic constant of ±0.00009. Also, the analysis does not take into account the ability to measure and remove errors in the null lens using a rotation test or the CGH null lens test.

5. NULL CORRECTOR CERTIFICATION WITH COMPUTER-GENERATED HOLOGRAMS

However apparently well made, there is always a small possibility that the null correctors can be flawed. If undetected, a null corrector error would result in the final shape of the mirror being incorrect. Two recent telescopes had their primary mirrors made to the wrong shape because of errors in the null correctors -- the Hubble Space Telescope[24] and the New Technology Telescope.[25] If accurate testing of the null correctors had been performed, the errors would have been discovered and corrected in the shop. Instead, the errors were not discovered until the finished mirrors were in their telescopes on a mountain top or in orbit.

An optical test using computer-generated holograms is planned to test and qualify the null correctors for the 6.5-m primary mirrors. The technique employs a rotationally symmetric computer-generated hologram (CGH) that tests the null corrector directly by synthesizing a wavefront that would be returned by a perfect primary mirror. The test, which is quick and highly accurate, has been demonstrated on null correctors for two 3.5-m primary mirrors[1,26].

5.1 DESCRIPTION OF CGH TEST OF NULL LENS

In the CGH null lens test, a custom manufactured hologram is illuminated by the laser light from the null lens. The hologram is made so it will diffract light back into the null corrector to appear as if it were a perfect primary mirror. The test is insensitive to alignment errors and uses no optics other than the hologram. Since the null corrector and CGH are fabricated independently, agreement between the two indicates a high probability that both are correct.

The hologram is simply a circular grating or zone plate fabricated onto a flat glass substrate. The CGH for the visible null test is fabricated using electron beam lithography that has been developed for the production of integrated circuits. The final hologram will be a relief grating with quarter-wave deep grooves and will be used at third order. The infrared hologram will be made using a less accurate and less-expensive optical writer. This CGH will use chrome rings on bare glass and be used at first order. For both tests, the required spacing of the rings is determined by the mirror surface that the hologram replaces and the laser wavelength. The groove depth and ring width are optimized to minimize fabrication costs, while giving the correct intensity of the diffracted light.

A layout of the CGH null test, shown in Fig. 12, depicts the null lens and CGH. No modifications are made to the null lens to perform this test. The null corrector tests the hologram exactly as if a real mirror was being measured.

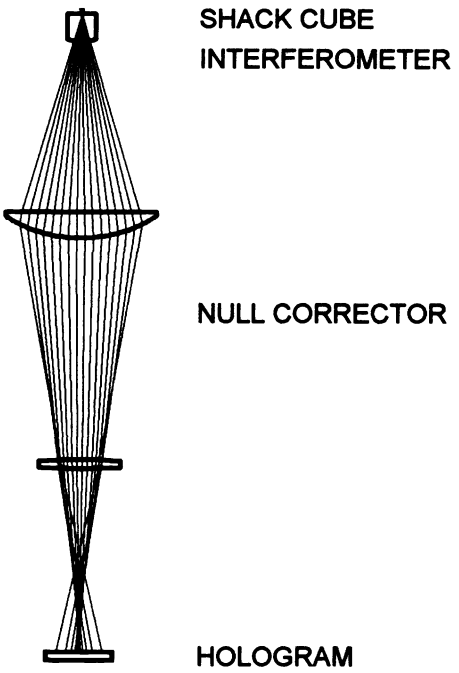

Figure 12. Layout of CGH test of null lens. The use of the CGH involves simply positioning the hologram at the correct location and making the measurement as if the mirror itself was being tested.

5.2 HOLOGRAM FABRICATION

The CGH null lens test is planned for all of the telescope projects at Steward Observatory. The computer-generated hologram for visible testing will be 136 mm in diameter and will consist of 12797 grooves, spaced as small as 4 μm. This is within the realm of existing lithographic technology, but it will be difficult and expensive to fabricate. This hologram will be directly e-beam written on the final substrate that is 7 inches square and 0.25 inches thick. This substrate will be polished flat to λ/10 as it is supported on a master flat. An error budget for this test indicates a measurement accuracy of ±40 ppm for the conic constant.[1]

A prototype of this hologram will be fabricated before the full CGH is made. This prototype, consisting of only a narrow diametrical slice across the circular hologram, will allow a test of the fabrication technique that requires only a small fraction of the cost of the full hologram. This diametrical slice will be useful for measuring spherical aberration in the null lens.

The accuracy requirements on the infrared hologram are not so severe, allowing it to be written on an optical writer. The infrared hologram will consist of 1928 chrome rings, with spacing as small as 13 μm. The pattern may be written using a writer developed at the Optical Sciences Center (University of Arizona) for the fabrication of chrome-on-glass zone plates for measuring convex aspheres up to 12 inches across.

6. CONCLUSION

The null correctors for the 6.5-m *f*/1.25 primary mirrors represent a significant advance in the field of metrology for large astronomical optics. The ability to fabricate null correctors, even for mild aspheres, is questioned by many astronomers. We have developed the techniques for designing, analyzing, fabricating, and certifying instruments for interferometric measuring large, fast primary mirrors. These null test instruments will provide rapid, accurate surface measurements to enable efficient stressed-lap figuring of the most challenging primary mirrors in the history of astronomy.

REFERENCES

1 J. H. Burge, *Advanced Techniques for Measuring Primary Mirrors for Astronomical Telescopes,* Ph. D. Dissertation, Optical Sciences, University of Arizona (1993).

2 A. Couder, "Procédé d'examen d'un miroir concave non-sphérique," Rev. Opt. Theor. Instrum., **6**,49-55 (1927).

3 H. E. Dall, "A null test for paraboloids," J. Br. Astron. Assoc. **57**, 201-205 (1947).

4 F. E. Ross, "Parabolizing mirrors without a flat," Astrophys. J. **98**, 341-346 (1943).

5 A. Offner, "A null corrector for paraboloidal mirrors," Appl. Opt **2**, 153-155 (1963).

6 R. T. Holleran, "An algebraic solution for the small lens null compensator," Appl. Opt. **7**, 137-144 (1968).

7 D. T. Puryayev. and N. S. Shandin, "Design of lens compensators for testing the concave astronomical mirrors of large telescopes," Sov. J. Opt. Technol. **46**, 207-209 (1979).

8 J. R. Moya. and J. E. A. Landgrave, "Third-order design of refractive Offner compensators,"Appl. Opt. **26**, 2667-2672 (1987).

9 J. M. Sasian, "Design of null lens correctors for the testing of astronomical optics," Opt. Eng. **27**, 1051-1056 (1988).

10 J. M. Sasian, "Optimum configuration of the Offner null corrector: testing an F/1 paraboloid," in *Surface Characterization and Testing II*, J. E. Greivenkamp and M. Young, eds., Proc. SPIE **1164**, 8-17 (1989).

11 C. E. DeVoe, "Limitations on aspheric surface testing with simple null correctors," Master Thesis, Optical Sciences Center, University of Arizona, Tucson, AZ (1989).

12 A. Offner, and D. Malacara, "Null tests using compensators," in *Optical Shop Testing,* D. Malacara, ed., (Wiley, New York, 1992) pp. 427-454.

13 D. Shafer, "Null lens design techniques," Appl. Opt. **31**, 2184-2188 (1992).

14 L. A. Selberg, "Interferometer accuracy and precision," in *Metrology; Figure and Finish*, B. Truax, ed., Proc. SPIE **749**, 8-18 (1987).

15 R. J. Wollensak and C. A. Rose, "Fabrication and test of 1.8-meter (71-inch) diameter, high-quality U.L.E.™ mirror," *The Space Telescope,* NASA SP-392, 123-134 (1976).

16 T. A. Facey, A. L. Nonnenmacher, D. P. Chadwick, "Fabrication of large aperture mirrors for astronomical telescopes," in *Advanced Technology Optical Telescopes IV,* L. D. Barr, ed., Proc. SPIE **1236**, 597-604 (1990).

17 H. M. Martin, J. H. Burge, and S. C. West, "Environmental effects in the testing of large astronomical mirrors," in *Precision Interferometric Metrology* (The American Society for Precision Engineering, Raleigh NC, 1992) Proc. ASPE **5**, pp. 72-75

18 B. Edlén,"The refractive index of air," Metrologia **2**, 71-80 (1966).

19 H. P. Stahl. and D. Ketelsen, "Aspheric figure generation using feedback from an infrared phase-shifting interferometer," in *Large Optics Technology*, G. M. Sanger, ed., Proc. SPIE **571**, 22-29 (1985).

20 R. V. Shack. and G. W. Hopkins, "The Shack interferometer," Opt. Eng. **18**, 226-228 (1979).

21 C. L. Koliopolis and D. S. Anderson, "High resolution phase measurements of optical surfaces," in *Ultraprecision Machining and Automated Fabrication of Optics*, D. L. Decker and R. A. Jones, eds., Proc. SPIE **676**, 90-93 (1986).

22 S. C. West, J. H. Burge, R. S. Young, D. S. Anderson, C. Murguic, D. A. Ketelsen, and H. M. Martin, "Optical metrology of two large highly aspheric telescope mirrors," Appl. Opt. **31**, 7191-7197 (1992).

23 J. M. Hill, "Optical design, error budget, and specifications for the Columbus Project Telescope," in *Advanced Technology Telescopes IV,* L. D. Barr, ed., Proc. SPIE **1236**, 86-107 (1990).

24 L. Allen, J. R. P. Angel, J. D. Mongus, G. A. Rodney, R. R. Shannon, C. P. Spoelhof, "The Hubble Space Telescope oprical systems failure report," NASA Report. Nov., 1990.

25 R. N. Wilson, F. Franza, L. Noethe, and G. Andreoni, "Active optics IV. Set up and performance of the optics of the ESO New Technology Telescope (NTT) in the observatory," J. Mod. Optics **38**, 219-243 (1991).

26 J. H. Burge, "Certification of null correctors for primary mirrors," in *Advanced Optical Manufacturing and Testing IV*, J. Doherty, Editor, Proc. SPIE **1994**, 248-259 (1993).